Supplemental material to: "Avalanche-like fluidization of a non-Brownian particle gel"

Aika Kurokawa, Valérie Vidal, Kei Kurita, Thibaut Divoux, and Sébastien Manneville

1 Supplemental movies

Five movies are provided as supplemental materials to Figs. 5–9 of the main text. All movies illustrate the temporal evolution of the global rheology and of the 1D and/or 2D velocity profiles recorded simultaneously to the rheology during successive avalanche-like events.

2 Supplemental figures

Supplemental Fig. 1(a) displays the evolution of the elastic and viscous moduli of the sample after preshear. The gel rebuilds quickly as evidenced by the fact that the elastic modulus is larger than the viscous modulus about 20 s after preshear has been stopped.

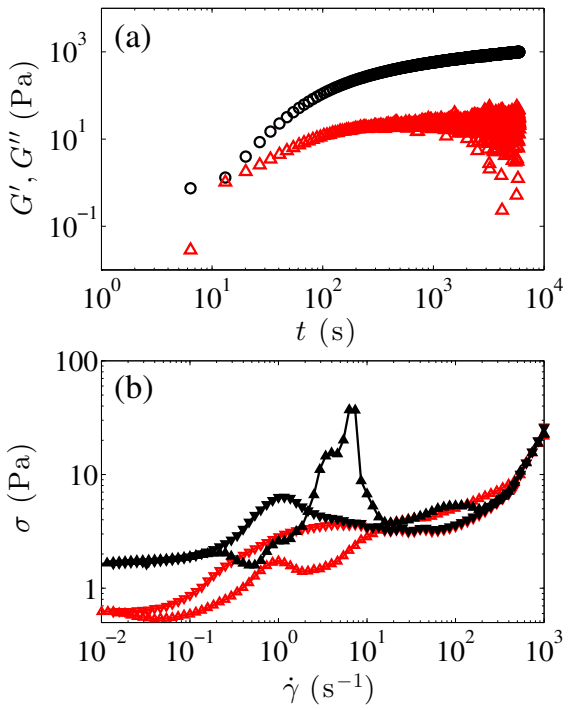

Fig. 1 (a) Elastic (○) and viscous moduli (△) vs time after a preshear at $\dot{\gamma}_p = 500$ s^{-1} for 2 min ($f = 1$ Hz, $\sigma = 0.05$ Pa). Same data as in Fig. 2(a) in the main text. (b) Flow curve, shear stress σ *vs.* applied shear rate $\dot{\gamma}$, obtained by decreasing (▽) and increasing (△) shear rate in order from 10^{-2} to 10^{3} s^{-1} with a waiting time of 8 s per point. Black (resp. red) symbols correspond to results in a smooth (resp. rough) geometry.

Supplemental Fig. 1(b) shows flow curves σ vs $\dot{\gamma}$ measured by rapidly sweeping down the shear rate from 10^3 to 10^{-2} s^{-1} and back up. The flow curves have complex non-monotonic shapes together with strong hysteresis under both smooth and rough boundary conditions.

Supplemental Fig. 2 illustrates the result of a frequency sweep performed at a constant strain ($\gamma = 0.5$ %) from 10 to 0.02 Hz, and for different aging times $t_w = 30$, 60 and 100 min after stopping the preshear. The elastic modulus G' is independent of the frequency and increases with the aging time t_w in agreement with Supplemental Fig. 1. The viscous modulus shows a broad minimum with no sign of increasing part at low frequencies, a feature that is typical of soft glassy systems [1].

Supplemental Fig. 3 shows the results of a strain sweep performed on the gel at a constant frequency $f = 1$ Hz for different aging times t_w after preshear. The gel yields at a constant strain of about 7 % that is roughly independent of the aging time t_w.

Supplemental Figs. 4 and 5 show the rheological and 2D-USV data obtained in smooth and rough boundary conditions

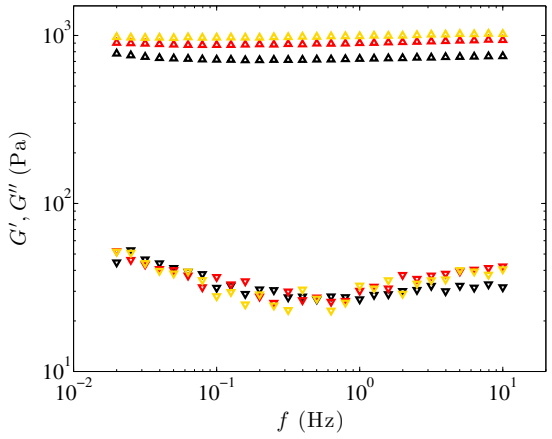

Fig. 2 Elastic (△) and viscous (▽) moduli vs frequency f. The frequency sweep is performed at a constant strain $\gamma = 0.5$ % and at different aging times t_w after preshear. [color, t_w (min)]: (–, 30); (–, 60); (–, 100).

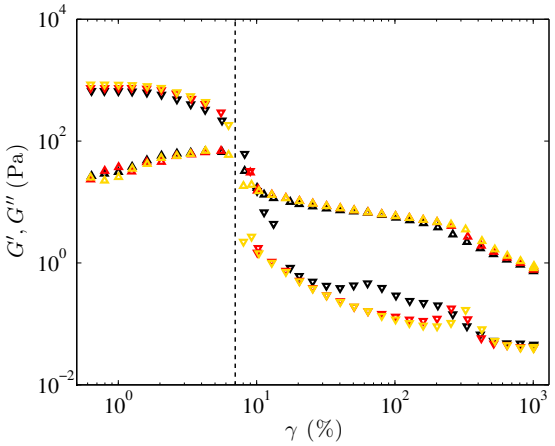

Fig. 3 Elastic (○) and viscous (△) moduli vs the strain amplitude. The strain sweep is performed at a fixed frequency $f = 1$ Hz with a waiting time of 8 s per point, and at different times t_w after the preshear. [color, t_w (min)]: (▬, 30); (▬, 60); (▬, 100). The vertical dashed line at $\gamma \sim 7$ % emphasizes the yield point defined as the point at which $G' = G''$.

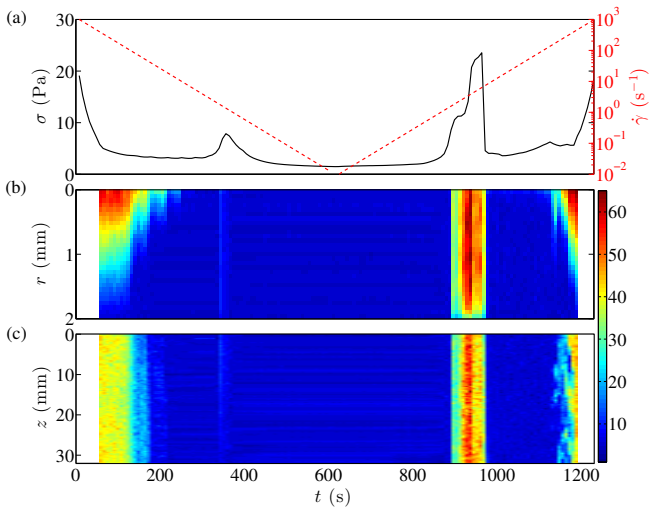

Fig. 4 Taylor-Couette cell with smooth boundary conditions. (a) Shear rate $\dot{\gamma}$ and shear stress σ vs time t obtained by first decreasing continuously $\dot{\gamma}$ from 10^3 to 10^{-2} s^{-1} in 75 logarithmically spaced points of duration $\delta t = 8$ s each, and then increasing $\dot{\gamma}$ over the same range. (b) Spatiotemporal diagram of the velocity data $v(r, z_0, t)$ as a function of the distance r to the rotor and time t, at $z_0 \simeq 15$ mm. (c) Spatiotemporal diagram of the velocity data $v(r_0, z, t)$ as a function of the vertical position z and time t, at $r_0 = 0.5$ mm. The vertical position z is measured from the upper boundary of the 2D-USV probe. The fluid velocity is color-coded in mm.s^{-1}.

respectively, by first decreasing the shear rate and then increasing it back again. The corresponding flow curves are shown in Fig. 1(b) of the present ESI. Here we also show spatiotemporal plots of the velocity profiles as a function of the radial position r at a given height ($z_0 \simeq 15$ mm) in the Taylor-Couette cell [Supplemental Figs. 4(b) and 5(b)], and as a function of the vertical position z, at a given radial position inside the gap ($r_0 = 0.5$ mm) [Supplemental Figs. 4(c) and 5(c)]. Velocity data are shown only for $\dot{\gamma}$ <460 and 340 s^{-1} in smooth and rough boundary conditions respectively, due to the limitation in the ultrasonic pulse repetition frequency to 20 kHz, which sets an upper bound on the measurable velocities[2].

For smooth boundary conditions, the flow curve exhibits a large hysteresis, mainly localized in a narrow range of shear rates [Supplemental Fig. 1(b)]. During the decreasing ramp of $\dot{\gamma}$, the sample which is first sheared homogeneously at large shear rates, enters a total wall slip regime at $t \simeq 200$ s, i.e., for $\dot{\gamma} \sim 20$ s^{-1} [Supplemental Fig. 4(b)]. This regime persists until $\dot{\gamma}$ is increased back up again. The subsequent fluidization of the material is abrupt and occurs in a narrow range of shear rates, $1 \lesssim \dot{\gamma} \lesssim 10$ s^{-1}, which coincides with the brutal increase of the global stress. Supplemental Fig. 4(b,c) reveal that the subsequent drop in the stress corresponds to flow arrest, i.e. total wall slip, until the sample fluidizes again for $\dot{\gamma} \gtrsim 100$ s^{-1} and that the local behavior of the sample is roughly homogeneous along the whole height of the cell during both ramps.

Supplemental Fig. 5 illustrates the exact same protocol as that reported in Supplemental Fig. 4, but performed in a rough Taylor-Couette cell. As also seen in Supplemental Fig. 1(b),

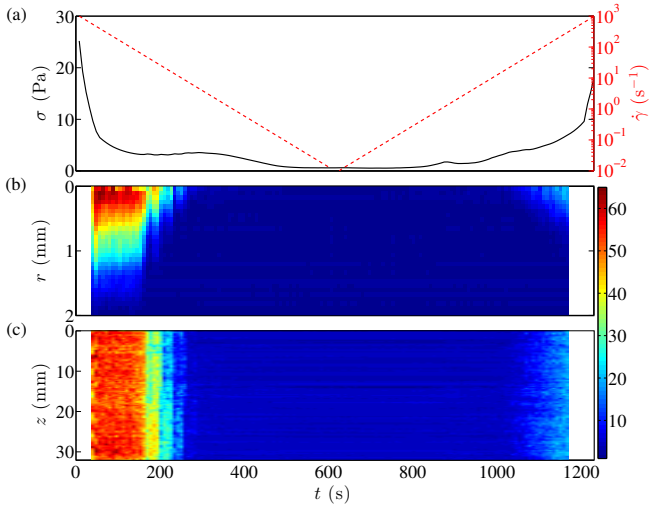

Fig. 5 Same as Supplemental Fig. 4 for a Taylor-Couette cell with rough boundary conditions.

the rheological hysteresis is far less pronounced in comparison to the data obtained with smooth boundary conditions. Here the flow remains homogeneous along the vertical axis during both ramps [Supplemental Fig. 5(c)]. The velocity profiles

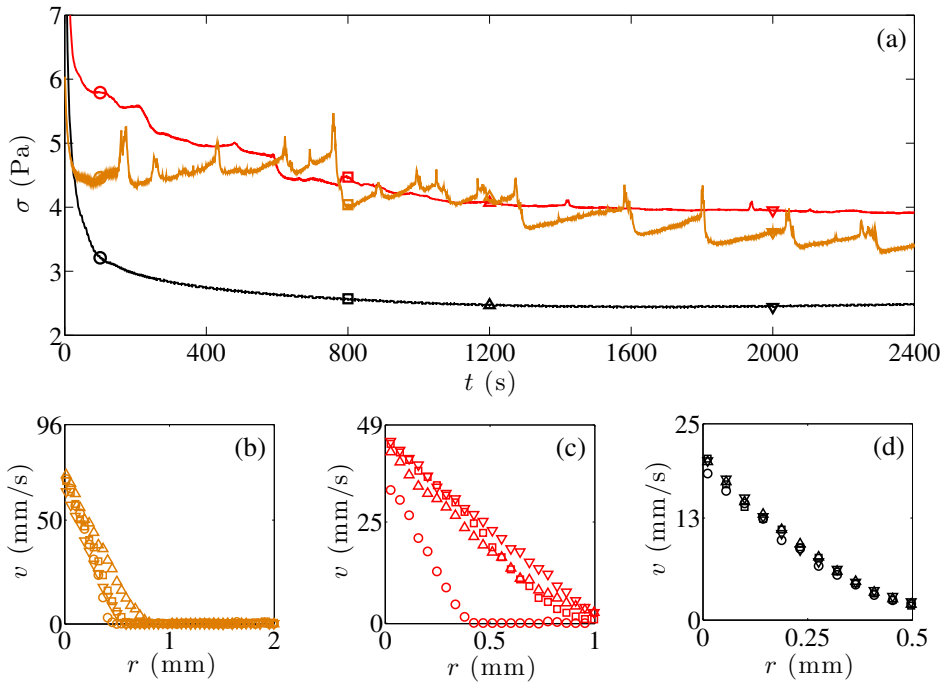

Fig. 6 (a) Stress response $\sigma(t)$ to a shear startup experiment performed at $\dot{\gamma} = 50$ s^{-1} for different gap sizes: [color, gap (mm)] = [—, 2], [—, 1], [—, 0.5]. (b)-(d) Velocity profile, where r is the distance to the rotor at different times in (a) [symbol, time (s)]: [◯, 100]; [□, 800]; [△, 1200]; [▽, 2000]. The rotor velocity corresponds to the upper bound of the vertical axis. The sample is aged during $t_w = 10$ min before each experiment.

at a given height in the Taylor-Couette cell also display very different behavior from the smooth case. In the decreasing ramp of $\dot{\gamma}$, the stress plateaus in between $\dot{\gamma} \sim 100$ s^{-1} and $\dot{\gamma} \sim 1$ s^{-1}, while shear localizes at the rotor. Below $\dot{\gamma} \sim 1$ s^{-1}, the stress displays a kink towards a second plateau, while the sample exhibits a plug flow. Increasing $\dot{\gamma}$ back up, the plug flow persists up to shear rates of a few 10 s^{-1}. Above the latter value, the fluidization of the sample proceeds from the rotor and involves transient banding. Full fluidization is not available in Supplemental Fig. 5(b) for the technical reason mentioned above.

Supplemental Fig. 6 shows the influence of the gap size on the fluid response to a shear startup experiment performed at $\dot{\gamma} = 50$ s^{-1} on a sample left at rest for $t_w = 10$ min. In a gap of size $e = 2$ mm, the same value as in the main text, the stress response displays a large number a peaks together with unsteady shear banding over 2400 s [Supplemental Fig. 6(b)]. Decreasing the size of the gap changes radically the sample behavior. In a gap twice as small ($e = 1$ mm), the stress response exhibits less peaks and the sample fluidizes entirely in about $t = 200$ s [Supplemental Fig. 6(c)]. Decreasing the gap by a factor of 4 ($e = 0.5$ mm) leads to a smooth stress response and to homogeneous velocity profiles from the beginning of the experiments, with significant slip at the moving boundary [Supplemental Fig. 6(d)].

References

1 T. G. Mason, J. Bibette and D. A. Weitz, *Phys. Rev. Lett.*, 1995, **75**, 2051–2054.

2 T. Gallot, C. Perge, V. Grenard, M.-A. Fardin, N. Taberlet and S. Manneville, *Rev. Sci. Instrum.*, 2013, **84**, 045107.